J Mater Sci (2010) 45:2340–2350
DOI 10.1007/s10853-009-4199-8

A fixed-grid numerical modelling of transient liquid phase bonding and other diffusion-controlled phase changes

J. F. Li · P. A. Agyakwa · C. M. Johnson

Received: 10 October 2009 / Accepted: 31 December 2009 / Published online: 20 January 2010

Abstract A transient liquid phase (TLP), in which a liquid layer is formed and subsequently solidifies, and other diffusion-controlled phase changes are generally associated with moving phase-change interfaces. Both fixed and variable grid discretization models have been formulated to investigate these diffusion-controlled problems. However, all numerical efforts to date have employed one of the approaches explicitly to track the moving interfaces across which there exist step changes in concentrations. In this article, the fixed-grid source-based method originally developed to simulate the temperature fields for melting-solidification phase change processes has been adopted to simulate diffusion-controlled dissolution and solidification. This method solves a unique diffusion equation for the different phases and the moving interfaces using implicit time integration. Compared with previously developed models, it is not only simpler in numerical formulation and procedure, but also more convenient to extend to many phases and high-dimensional problems. We report here the detailed formulation of the relevant equations, and compare and validate the model using experimental data and previous modelling predictions for several systems available from the existing literature.

List of symbols

a's	Coefficients in the numerical scheme
b	Parameter related to 'sensible mass density' at previous time step, and the 'latent mass density of phase change' at present time step in numerical scheme
D	Diffusion coefficient [m^2/s]
Δd	A small 'sensible mass density' interval used in numerical scheme [kg/m^3]
L	Half width of a TLP joint [m]
M	Sensible mass density [kg/m^3]
m	Mass fraction
ΔM	Latent mass density of phase change [kg/m^3]
s	Position of moving interface [m]
t	Time [s]
x	Position coordinate [m]

Greek symbols

ρ	Density [kg/m^3]

Superscript

0	Old value at previous time step
$'$	Specifies the corresponding dimensionless quantities

Subscript

0	Value associated with initial conditions
A	Phase A
B	Phase B
E, e	East neighbouring node
P	Node point
W, w	West neighbouring node

Introduction

Transient liquid phase (TLP) joints are formed when a low melting point depressant (MPD) in an interlayer, or called filler, diffuses into a surrounding bulk base metal, resulting in isothermal solidification [1]. Qualitatively, the physical

J. F. Li (✉) · P. A. Agyakwa · C. M. Johnson
Department of Electrical and Electronic Engineering,
The University of Nottingham, University Park,
Nottingham NG7 2RD, UK
e-mail: Jian.Li@nottingham.ac.uk

mechanisms behind TLP bonding have been well established [1, 2]. Bonding is controlled by the diffusion of solute and can be divided into four stages: dissolution, widening, isothermal solidification and homogenization. The TLP of an interlayer provides an effective way to fill up the gap between the surrounding base metals. After full processing, the final joint can be homogeneous in the form of a solid solution of the interlayer metal in the base metal. Therefore, TLP bonding can be carried out at relatively low processing temperatures whilst resulting in higher remelt temperatures of the produced joints [3–5]. This makes it promising in joining materials in a variety of industries. For example, it has received considerable attention as an alternative to the conventional soldering process for electronic interconnects that operate at high temperatures, e.g. above 125 °C [5–9].

Both analytical and numerical models based on Fick's diffusion equation have been widely developed to provide insight into the mechanisms of TLP bonding, as well as to optimize the bonding conditions and compositions [1, 2, 5, 10–18]. However, the analytical models have to be limited to a few idealized cases where analytical solutions are achievable. As a result, numerical models are generally required for providing more accurate and/or practically acceptable predictions. For numerical modelling of the TLP bonding process, there is generally a major difficulty associated with a moving phase-change interface, across which step changes in concentrations must be satisfied and whose locations are unknown *a-priori*.

Illingworth et al. [17] reviewed the work of numerical modelling of the TLP bonding process and outlined the approaches used to deal with the moving interface. Briefly, in the earliest fixed-grid discretization models, the diffusion equations were solved by imposing the requirement that the interface be located at one of the discretization nodes [5, 12]. In some later, more refined models [11, 13, 16], the equation for describing the motion of the moving interface was also discretized and solved simultaneously with the diffusion equations for the different phases. In the different efforts, the diffusion equations for the different phases could be solved either explicitly or implicitly, whilst the equation for tracking the moving interface had to be solved explicitly. In all these fixed-grid discretization models, either the constrained stepwise motion of the moving interface is physically unrealistic, or the size of the time step must be sufficiently small to generate convergent solutions. Furthermore, the discretization schemes reported in these models generally do not guarantee the conservation of the solute during the motion of the moving interface.

The problems of tracking the moving interface can be overcome using a variable grid discretization model developed by Illingworth et al. [17]. More recently, a similar variable grid discretization model was developed by Kajihara et al. [19] to simulate the diffusion-controlled phase changes, e.g. the migration behaviour of the γ/α interface due to isothermal carburization of the bcc-α phase in the binary Fe–C system. In this model, a different finite difference scheme was employed to discretize the diffusion equation and a different formulation was used to describe the flux balance at the migrating interface. In addition to the above finite difference models, locally re-defined mesh finite element model was also developed by Di Luozzo et al. [20] to simulate the TLP bonding of steel using an Fe–B interlayer. However, all these models still need to solve the equation describing the moving interface simultaneously with the diffusion equations for the different phases. As a consequence the extension of the models to many phases and high-dimensional problems can prove complex owing to the cumbersome formulation.

The mathematical equations for describing mass diffusion problems are analogous to those for describing the thermal diffusion phenomena. The fixed-grid source-based method is a standard approach and widely used in the numerical modelling of convection–diffusion melting-solidification phase change problems [21–26]. By introducing a scalar variable representing the liquid fraction and applying a source-based term, the unique continuity, momentum and energy equations can be solved for both liquid and solid phases; thereby, the major difficulty associated with a moving phase-change interface is overcome. Such a fixed-grid source-based method should be easily adopted, with slight modification, to solve mass diffusion phase change problems. In comparison with the previously developed numerical models, it should be much simpler and more convenient in the numerical formulation and procedure, in particular, to many phases and high-dimensional problems. To the authors' knowledge, however, no attempt has been made to use such a fixed-grid source-based method in modelling TLP bonding and other similar diffusion-controlled phase change processes.

In this study, we adopt the fixed-grid source-based method to model TLP bonding and other diffusion-controlled phase change processes. The main objective of this article is to demonstrate the validity and effectiveness of this method in comparison with the previous models [5, 10, 11, 17]. For this purpose, we will (i) derive the mathematical formulation into which the diffusion equations are modified in terms of those similar to the sensible enthalpy and latent heat of fusion in the corresponding energy equation, (ii) report the schemes used in the numerical procedures for achieving physically realistic solutions and for speeding up the calculation procedure, (iii) compare and validate the model using experimental data and previous modelling predictions for several material systems available from the existing literature and (iv) present a

further simplified formulation for parametric analysis of isothermal solidification during the TLP bonding process.

Modelling

Mathematical description of the problem

As in the previous models [5, 10, 11, 17], the one-dimensional diffusion-controlled, two-phase and moving interface problem is considered in the current model, see Fig. 1. In order for the change of Molar volume of the solute in the different phases to be further taken into account, the governing equations are given in terms of mass fraction by:

$$\frac{\partial \rho(x,t)m(x,t)}{\partial t} = \frac{\partial}{\partial x}\left[D_{\mathrm{A}}\frac{\partial \rho(x,t)m(x,t)}{\partial x}\right], \quad 0<x<s(t) \tag{1}$$

$$\frac{\partial \rho(x,t)m(x,t)}{\partial t} = \frac{\partial}{\partial x}\left[D_{\mathrm{B}}\frac{\partial \rho(x,t)m(x,t)}{\partial x}\right], \quad s(t)<x<L \tag{2}$$

$$-D_{\mathrm{A}}\frac{\partial \rho(x,t)m(x,t)}{\partial x}\bigg|_{x=s(t)^-} + D_{\mathrm{B}}\frac{\partial \rho(x,t)m(x,t)}{\partial x}\bigg|_{x=s(t)^+} = [\rho_{\mathrm{A}}m_{\mathrm{A}} - \rho_{\mathrm{B}}m_{\mathrm{B}}]\frac{\partial s(t)}{\partial t}, \quad x = s(t) \tag{3}$$

They are subject to the following boundary conditions:

$$\frac{\partial \rho(x,t)m(x,t)}{\partial x} = 0 \quad x = 0 \tag{4a}$$

$$\frac{\partial \rho(x,t)m(x,t)}{\partial x} = 0 \quad x = L \tag{4b}$$

And the initial conditions can be given as:

$$\rho(x,0)m(x,0) = \rho_{\mathrm{A0}}m_{\mathrm{A0}}, \quad 0 \le x \le s(0) \tag{5a}$$

$$\rho(x,0)m(x,0) = \rho_{\mathrm{B0}}m_{\mathrm{B0}}, \quad s(0) \le x \le L \tag{5b}$$

If constant Molar volume is assumed, Eqs. 1–3 can be readily reduced to those in terms of Molar fraction as given in the previous models [5, 10, 11, 17].

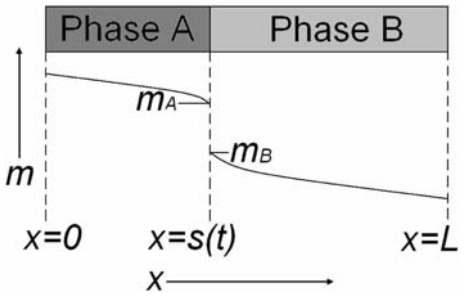

Fig. 1 Schematic illustration of the profile of mass fraction across half of a TLP joint at the instant time of t. The other half from $x = -L$ to $x = 0$ is symmetrical

Similar to the sensible enthalpy and latent heat of fusion in the energy equation for describing the phase change of melting and solidification [21–26], we may define a so-called 'sensible mass density' as:

$$M(x,t) = \rho(x,t)m(x,t) - \Delta M \tag{6}$$

and a 'latent mass density of phase change' as:

$$\Delta M = \begin{cases} (\rho_{\mathrm{A}}m_{\mathrm{A}} - \rho_{\mathrm{B}}m_{\mathrm{B}}), & \rho(x,t)m(x,t) \ge \rho_{\mathrm{A}}m_{\mathrm{A}} \\ 0, & \rho(x,t)m(x,t) \le \rho_{\mathrm{B}}m_{\mathrm{B}} \end{cases} \tag{7}$$

Then Eqs. 1–3 can be transformed into a unique equation for the two phases and the moving interface:

$$\frac{\partial M(x,t)}{\partial t} = \frac{\partial}{\partial x}\left(D(x,t)\frac{\partial M(x,t)}{\partial x}\right) - \frac{\partial \Delta M}{\partial t}, \quad 0<x<L \tag{8}$$

with the boundary conditions:

$$\frac{\partial M(x,t)}{\partial x} = 0 \quad x = 0 \tag{9a}$$

$$\frac{\partial M(x,t)}{\partial x} = 0 \quad x = L \tag{9b}$$

and the initial conditions:

$$M(x,0) = \rho_{\mathrm{A0}}m_{\mathrm{A0}} - \Delta M, \quad 0 \le x \le s(0) \tag{10a}$$

$$M(x,0) = \rho_{\mathrm{B0}}m_{\mathrm{B0}}, \quad s(0) \le x \le L \tag{10b}$$

Equation 8 is essentially the same as the energy equation that takes account of heat conduction only for describing the phase change of melting and solidification and expressed in terms of sensible enthalpy. Here, the 'sensible mass density', 'latent mass density of phase change' and diffusion coefficient are used to replace the sensible enthalpy, latent heat of fusion and thermal diffusivity in the energy equation. Equations 6–10 formulate the mathematical description of the current model for TLP bonding and other similar diffusion-controlled phase change process. They are the main contribution of this study and are readily solved using the fixed-grid source-based method [21–26].

Numerical procedures

Discretizing the coordinate x into a fixed grid consisting of N nodes, the governing equation and boundary conditions formulated in Eqs. 6–10 are solved using the volume-controlled finite-difference method outlined by Patankar [27]. The governing equation, Eq. 8, is discretized using the fully implicit discretization scheme:

$$a_P M_P = a_E M_E + a_W M_W + b \tag{11}$$

where the subscripts, P, E and W, indicate the appropriate nodal values, the 'a' terms are coefficients dependent on the fluxes of the 'sensible mass density' and the 'latent mass density of phase change' into the Pth control volume,

and the parameter, b, includes the terms associated with the evaluation of 'sensible mass density' at the previous time step, and the 'latent mass density of phase change'. The terms related to the 'latent mass density of phase change' are discretized according to the following expression:

$$\frac{\partial \Delta M}{\partial t} = \frac{\Delta M(M_P) - \Delta M(M_P^0)}{\Delta t} = \begin{cases} 0, & M_P^0 < \rho_B m_B, M_P < \rho_B m_B \text{ or } M_P^0 > \rho_B m_B + \Delta d, M_P > \rho_B m_B + \Delta d \\ \frac{k(M_P)}{\Delta t} M_P - \left[\frac{k(M_P)}{\Delta t}\rho_B m_B + \frac{\Delta M(M_P^0)}{\Delta t}\right], & \text{Otherwise} \end{cases} \tag{12}$$

where the superscript, 0, indicates the nodal value at the previous time step, and:

$$\Delta M(M_P) = \begin{cases} (\rho_A m_A - \rho_B m_B)\min\left(\frac{M_P - \rho_B m_B}{\Delta d}, 1\right), & M_P > \rho_B m_B \\ 0, & M_P \le \rho_B m_B \end{cases} \tag{13}$$

$$k(M_P) = \begin{cases} \frac{\rho_A m_A - \rho_B m_b}{\max(\Delta d, M_P - \rho_B m_B)}, & M_P > \rho_B m_B \\ 0, & M_P \le \rho_B m_B \end{cases} \tag{14}$$

where a small 'sensible mass density' interval, e.g. $\Delta d = 1.0 \times 10^{-4}$ to 1.0×10^{-10} g/cm^3 depending on a particular simulation case, is employed to describe the diffusion-controlled phase change.

During numerical iteration, $\Delta M(M_P)$ and $k(M_P)$ are updated according to the nodal 'sensible mass density' obtained at the previous iteration step. This numerical scheme is somewhat different from that used in the standard fixed-grid source-based method, where the latent heat of fusion is directly updated using an appropriate formulation of the latent heat function [21–26]. In the present case, the 'latent mass density of phase change' has been linearized using Eq. 14, which was found to speed up the convergence of the iteration significantly.

With Eq. 12 and referring to Fig. 2, the 'a' coefficients and the 'b' parameter in Eq. 11 are given by:

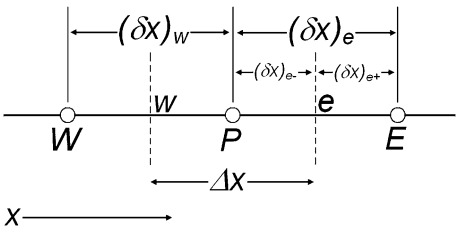

Fig. 2 Grid-point cluster and the relevant geometric parameters

$$a_E = \frac{D_e}{(\delta x)_e} \tag{15a}$$

$$a_W = \frac{D_w}{(\delta x)_w} \tag{15b}$$

$$b = \frac{\Delta x}{\Delta t}\left[k(M_P)\rho_B m_B + \Delta M(M_P^0) + M_P^0\right] \tag{15c}$$

$$a_P = a_E + a_W + \frac{\Delta x}{\Delta t}[1 + k(M_P)] \tag{15d}$$

where the diffusion coefficients, D_e and D_w at the boundaries of a control volume should be the harmonic mean, rather than the arithmetic mean, as described in detail in Ref. [27]. Also, it is important to take a similar approach for updating the diffusion coefficient for any node whose 'sensible mass density' is between $\rho_B m_B$ and $\rho_B m_B + \Delta d$ as:

$$D_P = \left[\frac{f_A}{D_B} + \frac{1 - f_A}{D_A}\right]^{-1} \tag{16}$$

where

$$f_A = \frac{M_P - \rho_B m_B}{\Delta d} \tag{17}$$

Otherwise, the simulation result may be physically unrealistic. For each step of the iteration procedure, the group of discretized equations for all the nodes is solved using the standard TriDiagonal-Matrix Algorithm [27]. Within each time step, calculation convergence was verified after the absolute residues of all the 'sensible mass density' values were four orders of magnitude lower than the selected small 'sensible mass density' interval, Δd. Once the converged 'sensible mass density' values are obtained, the moving interface of the two phases is calculated using the following reverse function:

$$s_1(t) = x|_{M(x,t)=\rho_B m_B} = M^{-1}(\rho_B m_B, t) \tag{18}$$

In addition, another moving interface expressed as

$$s_2(t) = x|_{M(x,t)=\rho_B m_B + \Delta d} = M^{-1}(\rho_B m_B + \Delta d, t) \tag{19}$$

is also calculated and compared with the interface $s_1(t)$. In this study, they are both determined using linear

Table 1 Simulation cases and the corresponding input parameters

Simulation case	Ni/Ni–P		α-brass/β-brass		Au/Sn			
	A1	A2	B1	B2	C1	C2	C3	C4
$s(0)$ (μm)	12.5	12.5	190.5	381	0.5	0.5	0.5	0.5
m_{A0} (wt%)	11.02	11.02	40.08	40.08	100	100	100	100
ρ_{A0} (g/cm^3)	8.10	8.93	9.02	9.02	11.63	7.31	7.31	7.31
m_A (wt%)	5.67	5.67	37.56	37.56	19.27	19.27	19.27	19.27
ρ_A (g/cm^3)	8.47	8.95	9.02	9.02	17.12	14.66	17.12	14.66
D_A (μm^2/s)	500.0	500.0	140.0	140.0	22.92	22.92	22.92	22.92
L (μm)	3012.5	3012.5	565	755.5	5.5	5.5	5.5	5.5
m_{B0} (wt%)	0.0	0.0	29.69	29.69	0.0	0.0	0.0	0.0
ρ_{B0} (g/cm^3)	8.90	8.90	8.99	8.99	19.30	19.30	19.30	19.30
m_B (wt%)	0.088	0.088	33.13	33.13	11.07	11.07	11.07	11.07
ρ_B (g/cm^3)	8.90	8.90	9.00	9.00	17.99	17.99	17.99	16.33
D_B (μm^2/s)	18.0	18.0	2.5	2.5	0.23	0.23	0.23	0.23
Reference	[11, 17, 28]		[10, 11, 17, 28]		[5, 28, 29]			

interpolation of the nodal 'sensible mass density' values. With the exception that the average mass density of a material system is between $\rho_A m_A$ and $\rho_B m_B$, $s_1(t)$ and $s_2(t)$ should be very close to each other. Otherwise, as presented below, a reduced small 'sensible mass density' interval, Δd, or an increased number of nodes, should be employed for achieving solutions which reasonably reflect the mass density step change at the moving interface. However, this generally requires more computation effort.

The simulation cases for three material systems, TLP bonding of Ni/Ni–P, solid state diffusion of α-brass/β-brass and TLP bonding of Au/Sn systems, are listed in Table 1 [5, 10, 11, 17, 28, 29]. All calculations were executed using self-written codes of the MATLAB R12 (The Mathworks, Inc.) on a PC computer with Intel[R] Pentium[R] 4 CPU 2.80 GHz processor and 504.0 MB RAM. The run time depended on the material system, the simulation case, the number of nodes, the small 'sensible mass density' interval and the time step. The number of nodes ranged from 50 to 5,000, the small 'sensible mass density' interval, Δd, from 1.0×10^{-4} to 1.0×10^{-10} g/cm^3, and the variable time step, Δt, from 0.0001 to 5 s were used for the different simulation cases. The running times were in the range of several minutes to 1 h for all the simulation cases for achieving reasonable accuracy.

Results, validation and discussion

TLP bonding of Ni/Ni–P

TLP bonding of base metal pure nickel using Ni–19at.%P as an interlayer was both experimentally and numerically investigated by Zhou and North [11]. The experimental result was also used by Illingworth et al. [17] to validate their variable grid model. In the previous models, Zhou and North, and Illingworth et al. [11, 17] both assumed a constant Molar volume irrespective of phase and composition. In this study, this assumption is first reserved using the input parameters of the simulation case, Case A1, in Table 1, to investigate the effects of the number of grid nodes and the size of the small 'sensible mass density' interval, Δd, on the simulation result. Note that it is the ratio, rather than the absolutes of the densities of the two phases that determine whether the Molar volume of the solute changes in the two phases. As shown in Figs. 3 and 4, both coarse grid system and large 'sensible mass density' interval lead to a relatively wide spatial zone between the interfaces $s_1(t)$ and $s_2(t)$. Careful observation reveals that the mechanisms behind the effects of the number of grid nodes and the size of the small 'sensible

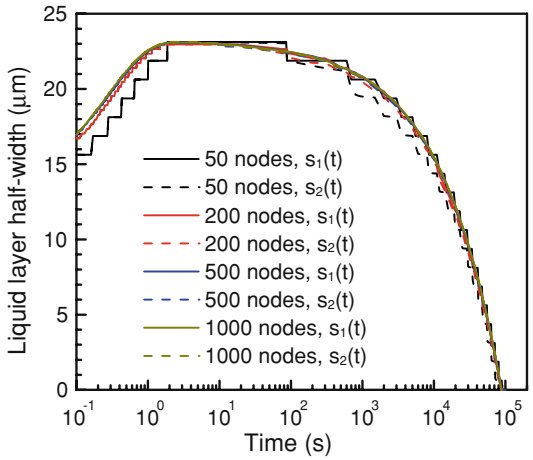

Fig. 3 Predicted evolution of liquid layer half-width versus bonding time using a small 'sensible mass density' interval of 1.0×10^{-8} g/cm^3 for TLP bonding of the Ni/Ni–P system, showing the effect of the number of grid nodes

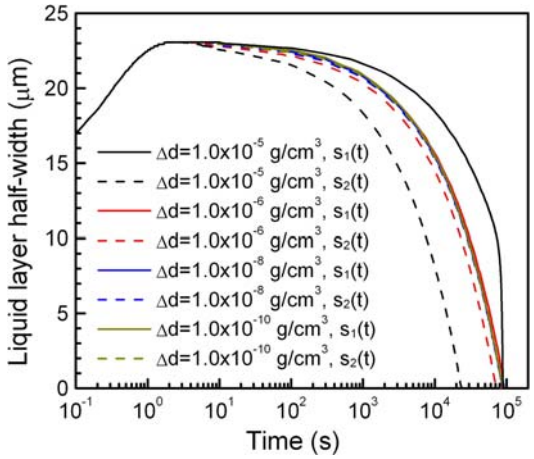

Fig. 4 Predicted evolution of liquid layer half-width versus bonding time using a grid system of 500 nodes for TLP bonding of the Ni/Ni–P system, showing the effect of a small 'sensible mass density' interval

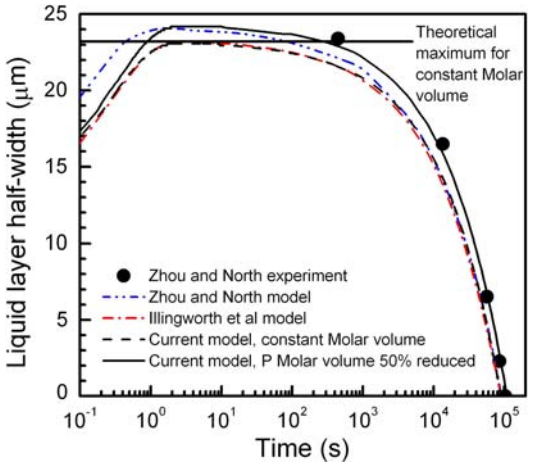

Fig. 5 Predicted evolution of liquid layer half-width versus bonding time for TLP bonding of the Ni/Ni–P system in comparison with previous experiments and modelling predictions [11, 17]. In the current model, a small 'sensible mass density' interval of 1.0×10^{-8} g/cm^3 and a grid system of 500 nodes are employed

mass density' interval are different. For the coarse grid system, the relatively wide spatial zone is caused by the present algorithm for determining the interfaces, the linear interpolation of the nodal 'sensible mass density' values. For large 'sensible mass density' interval, the relatively wide spatial zone is a result of the spatial distribution of the simulated 'sensible mass density'. Nevertheless, once the number of the grid nodes is larger than 500 and the 'sensible concentration' interval is smaller than 1.0×10^{-8} g/cm^3, $s_1(t)$ and $s_2(t)$ almost overlap with each other during the entire dissolution and solidification stages.

Under the assumption of constant Molar volume, the current fixed-grid source-based model predicts the evolution of liquid layer half-width against bonding time, in good agreement with that predicted from Illingworth et al.'s [17] variable grid model, see Fig. 5. The theoretical maximum liquid layer half-width of 23.2 μm was calculated from the equilibrium concentration of the solute, 10.233 at.% (equivalent to the current 8.47 wt% in Table 1), by ignoring any diffusion of the solute into the solid [17]. The predictions of both the current model and Illingworth et al.'s model did not exceed the theoretical maximum. As pointed out by Illingworth et al. [17], the predictions of Zhou and North's [11] fixed-grid model exceeded the theoretical maximum, indicating that their simulation violated the conservation of the solute.

One experimental datum is greater than the theoretical maximum. Illingworth et al. [17] explained this from two possibilities. The first is that the assumption of constant Molar volume in the liquid may be incorrect. The second possibility is that fluid flow during the experiments may have affected the thickness of the liquid layer and the diffusion. The current authors tend towards the first explanation rather than the second. This is because fluid flow generally speeds up mass transfer and makes the mass density more uniform within the liquid; however, this does not produce a situation in which the mass fraction of the solute is reduced beyond the equilibrium mass fraction. Phosphorous is an interstitial element in solid nickel. If we assume a 50% reduction in the Molar volume of phosphorous and keep the other conditions unchanged, we may use the parameters of Case A2 in Table 1 as inputs into the current fixed-grid source-based model. As also shown in Fig. 5, this produces a simulation result more closely consistent with experimental data. Such a result demonstrates that the reduction in Molar volume of phosphorous is probably the real reason for the experimental datum being greater than the theoretical maximum based on the constant Molar volume.

Under the assumption of constant Molar volume, both the current fixed-grid source-based model and Illingworth et al.'s variable grid model have similar prediction accuracy. However, the current model does provide some advantages, in particular the mathematical formulation and the relevant numerical procedure are relatively simple. They can be more easily extended to multi-component, multi-phase systems and high-dimensional problems, without the need for tracing a number of moving interfaces of the different phases. It is also convenient to incorporate convection caused by fluid flow and other physical phenomena into the model when necessary. These are extremely useful in numerical simulations for complex systems, e.g. liquid sintering of mixed powders and grain growth in polycrystalline materials [30, 31].

Solid state diffusion of α-brass/β-brass

The solid diffusion of Zn in α-brass/β-brass couples at 870 °C was first investigated by Heckel et al. [10]. Experimental data were used to validate the numerical models developed by the aforementioned authors [10] and other investigators [11, 17]. In these numerical models, both fixed-grid and variable grid schemes were employed. As pointed out by Illingworth et al. [17], the numerical predictions were significantly dependent on user-specified diffusion coefficients. The best prediction was achieved by Illingworth et al.'s variable grid model using the following diffusion coefficients: D_α = 2.5 μm^2/s and D_β = 140.0 μm^2/s.

The experimental diffusion couples consisted of alternative multi-layers of α-brass and β-brass. A constant initial thickness of α-brass, 749 μm, and two different initial thicknesses of β-brass, 381 and 762 μm, were employed. The initial Molar fractions of Zn in the α-brass and β-brass were 39.4 and 36.9 at.%, and the equilibrium Molar fractions of Zn at the interface terminals of the two phases were 32.5 and 29.1 at.%, respectively. These thermodynamic and geometric parameters are changed into the corresponding parameters of simulation cases, Case B1 and Case B2 under the assumption of constant Molar volume in Table 1, to input the current model. The interface displacements were then calculated from the simulation results of the mass density distributions. Again, the current fixed-grid source-based model provides predictions closely consistent with those of Illingworth et al.'s variable grid model, as can be seen from Fig. 6.

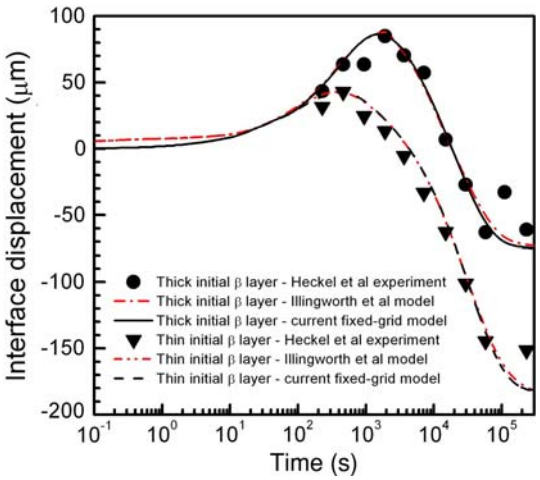

Fig. 6 Predicted interface displacement as a function of treatment time for α-brass/β-brass couples at 870 °C in comparison with previous experiments and modelling predictions [10, 17]. In the current model, a small 'sensible mass density' interval of 1.0×10^{-6} g/cm^3, and grid systems consisting of 565 nodes and 755 nodes are employed for the thin and thick initial β layers, respectively

TLP bonding of Au/Sn

The TLP bonding of Au/Sn was investigated by Cain et al. using a fixed-grid numerical model [5]. In their model, the diffusion was characterized by the diffusion coefficient of Sn in Au, and the formation of the various intermetallic compounds was ignored. The diffusion equation in terms of Molar fraction for the solid phase was solved by imposing the requirement that the moving interface was at one of the discretization nodes, whilst the thickness of the liquid phase was determined by assuming mass balance and a certain distribution of solute concentration within the liquid layer.

The TLP bonding of a 5-μm thick Au layer in contact with a 1-μm thick Sn middle layer at 300 °C is simulated using the current fixed-grid source-based model. The initial and interfacial mass fractions are calculated using the corresponding values of Molar fractions, and the diffusion coefficients reported by Cain et al. [5] are employed. However, several combinations of the constant and variable Molar volumes of Sn and Au in the liquid and solid phases are considered. As listed in Table 1, Case C1 specifies constant Molar volume. Case C2 describes a situation where both Sn and Au keep the Molar volumes of their corresponding pure components in the liquid phase, and at the same time have the same Molar volume as the pure Au in the solid phase. Case C3 slightly modifies the description of Case C2; the Molar volume of Sn gradually changes to the Molar volume of Au with the mass fraction approaching the interface equilibrium value. Case C4 states a situation where both Sn and Au have their Molar volumes of the corresponding pure components no matter whether they are in the liquid or solid phase. Amongst the four cases, Case C3 is closest to the physical description of Cain et al. [5] model. The resulting evolution of liquid layer half-width against bonding time for the four cases are compared with Cain et al.'s prediction, see Fig. 7. It is easily understood that the predicted maximum liquid half-width of the current model for Case C3 is slightly lower than Cain et al.'s prediction. This can be attributed to the fact that some Sn atoms have diffused into the Au base metal layer before the liquid layer reaches the maximum thickness. In the physical description of Cain et al.'s model, the maximum thickness of the liquid layer was calculated from the equilibrium Molar fraction of Sn by ignoring any diffusion of Sn atoms into the Au base metal layer. However, the bonding times at which the liquid phase disappears predicted from the current model for the four simulation cases are all significantly shorter than that predicted from Cain et al. [5] model.

It requires a stepwise motion of the moving interface if the moving interface is imposed at one of the discretization nodes. As pointed out by Illingworth et al. [17], this is

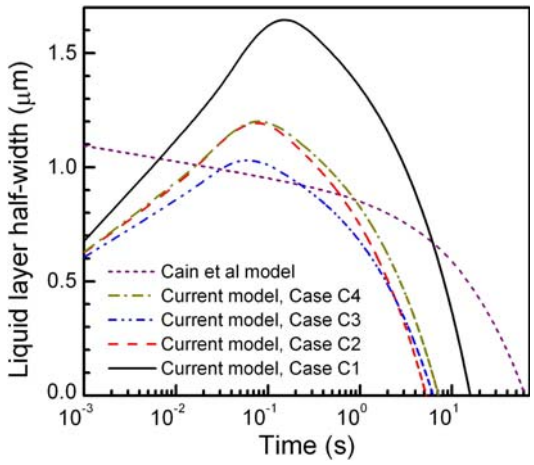

Fig. 7 Predicted evolution of liquid layer half-width versus bonding time for TLP bonding of the Au/Sn system in comparison with Cain et al.'s prediction [5]. In the current model, a small 'sensible mass density' interval of 1.0×10^{-4} g/cm^3 and a grid system of 1,100 nodes are employed

physically unrealistic, and probably introduced significant errors into the model. Such an argument agrees well with the comparison of the current predictions with Cain et al.'s prediction in Fig. 7. Cain et al. presented a predicted solidification curve that was in reasonable agreement with the experimental data of two samples [5]. However, on the one hand, no detail about the sample geometry was given, and the agreement may be just a coincidence. On the other hand, the phase diagram of the Au–Sn binary system is quite complicated [29]. TLP bonding at 300 °C would involve the formation and transformation of a series of intermetallic compounds (IMCs), i.e. ε, δ, ζ and β phases. This is far more complicated than the physical description of the diffusion of a solute in a two-phase system. Therefore, the validity of Cain et al.'s model is questionable. The formation and transformation of these IMCs can be easily incorporated into the current model. However, this has not been attempted as a result of a lack of reliable data on diffusion coefficients for these IMCs.

Parametric analysis of isothermal solidification during TLP bonding

For the TLP bonding of the different material systems, the times of dissolution and widening, i.e. the times from the beginning to the moment at which the maximum liquid layer widths are reached, are all negligible when compared with the subsequent times of the isothermal solidification. Because the diffusion coefficient of the solute in the liquid phase is normally several orders of magnitude higher than that in the solid phase, we may assume that the isothermal solidification starts at the point where the amount of the solute diffused into the solid phase is ignored and the liquid layer has the maximum width with the equilibrium mass fraction of the solute. Under such an assumption, the diffusion coefficient of the solute in the liquid phase can be taken as any value, e.g. the same value as the diffusion coefficient of the solute in the solid phase. If the latter is further assumed as constant, then Eq. 8 can be changed into the dimensionless form for describing the isothermal solidification during TLP bonding:

$$\frac{\partial M'(x',t')}{\partial t'} = \frac{\partial M'^2(x',t')}{\partial x'^2}) - \frac{\partial \Delta M'}{\partial t'}, \quad 0 < x' < L' \tag{20}$$

where the corresponding dimensionless quantities are defined by:

$$\Delta M'(M'_P) = \begin{cases} \min\left(\frac{M'_P - M'_B}{\Delta d'}, 1\right), & M'_P < M'_B \\ 0, & M'_P \geq M'_B \end{cases} \tag{21}$$

$$M'_{\mathrm{B}} = \frac{\rho_{\mathrm{B}} m_{\mathrm{B}} - \rho_{\mathrm{B0}} m_{\mathrm{B0}}}{\rho_{\mathrm{B}} m_{\mathrm{B}} - \rho_{\mathrm{A}} m_{\mathrm{A}}} \tag{22}$$

$$t' = \frac{Dt}{s^2(0)} \tag{23}$$

$$x' = \frac{x}{s(0)} \tag{24}$$

$$M'(x',t') = \frac{M(x,t) - \rho_{\mathrm{B0}} m_{\mathrm{B0}}}{\rho_{\mathrm{B}} m_{\mathrm{B}} - \rho_{\mathrm{A}} m_{\mathrm{A}}} \tag{25}$$

Correspondingly, the dimensionless boundary conditions are given by:

$$\frac{\partial M'(x',t')}{\partial x'} = 0, \quad x' = 0 \tag{26a}$$

$$\frac{\partial M'(x',t')}{\partial x'} = 0, \quad x' = \frac{L}{s(0)} \tag{26b}$$

and the dimensionless initial conditions are given by:

$$M'(x',0) = \frac{\rho_{\mathrm{B}} m_{\mathrm{B}} - \rho_{\mathrm{B0}} m_{\mathrm{B0}}}{\rho_{\mathrm{B}} m_{\mathrm{B}} - \rho_{\mathrm{A}} m_{\mathrm{A}}} + \Delta d', \quad 0 \leq x' \leq 1 \tag{27a}$$

$$M'(x,0) = 0, \quad 1 \leq x' \leq \frac{L}{s(0)} \tag{27b}$$

The above-derived dimensionless diffusion equation and the corresponding boundary and initial conditions can be used for parametric analysis of isothermal solidification during TLP bonding. From Eqs. 20 to 27, it is clear that the process of isothermal solidification is dependent on only a sub-saturation parameter, $M'(x',0)$, and a geometric parameter, $L/s(0)$. The diffusion coefficient, D, and the initial thickness of the liquid layer, $s(0)$, affect the solidification in a self-similar manner. The solidification time increases linearly with increasing diffusion coefficient, and parabolically as the initial thickness of the liquid layer increases. If the mass fractions in the Eqs. 20, 25 and 27 are transformed into Molar fractions, the current results are

the same as those derived by Illingworth et al. [18] using the variable grid model. In the latter model, two diffusion equations in terms of Molar fraction, one for the solid phase and the other one for the moving interface, were employed, and hence the sub-saturation parameter was expressed in terms of Molar fraction.

Equations 20–27 can also be considered as the formulation of a simplified model for isothermal solidification during TLP bonding. They are readily solved using the same numerical procedure expressed by Eqs. 11–19 that are used for solving Eqs. 6–10 of the current full model. The simulation results for the evolution of the dimensionless width versus dimensionless time for three sub-saturation parameters, $M'(x',0)$, and different geometric parameters, $L/s(0)$, are presented in Fig. 8. They are also in good agreement with those predicted from Illingworth et al.'s [18] variable grid model. This further verifies that the current fixed-grid source-based model does not have the problems associated with the convergence of calculation and conservation of solute in previous fixed-grid models, as pointed out by Illingworth et al. [17].

We also simulated isothermal solidification for the four cases of the Au/Sn system listed in Table 1 using the simplified model. The simulation results of the dimensionless liquid layer half-widths and dimensionless bonding times are changed back to the real liquid layer half-widths and the real bonding times, and are compared with those predicted using the current full model. As shown in Fig. 9, the maximum liquid half-widths predicted from the simplified model are all slightly higher than those predicted from the full model. This can be easily ascribed to the fact some Sn atoms would have diffused into the Au base metal before isothermal solidification starts in the full model. On the other hand, predictions of the bonding times at which the liquid layer disappears using both the full and the simplified model are almost the same for the four simulation cases. These results indicate that the simplified model can provide a reasonable approximation to replace the full

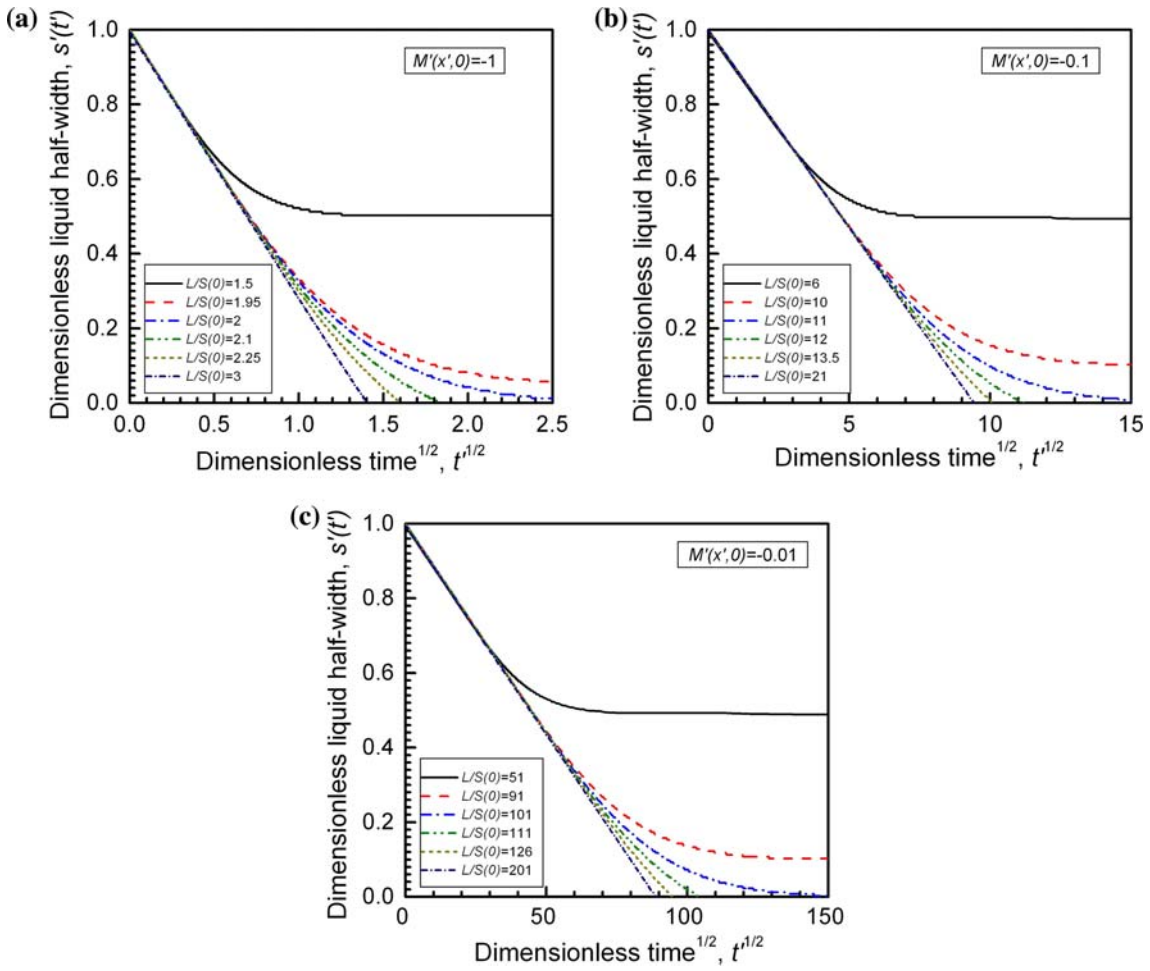

Fig. 8 Predicted evolution of dimensionless liquid layer half-width versus dimensionless bonding time for TLP bonding with three sub-saturation parameters, $M'(x',0)$, and different geometric parameters, $L/s(0)$. A dimensionless small 'sensible mass density' interval, $\Delta d'$, of 1.0×10^{-10} and grid systems of 500 to 1,000 nodes are employed for the simplified model

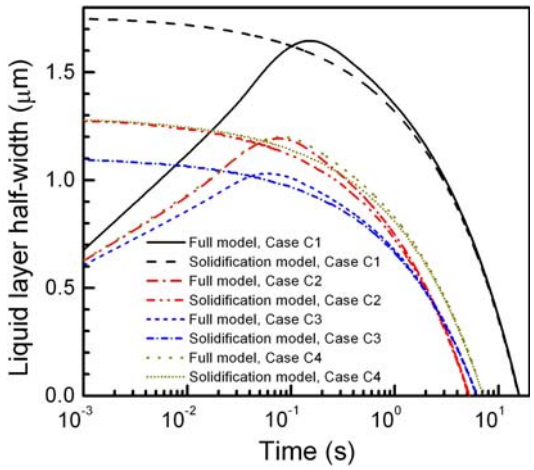

Fig. 9 Comparison of the predictions from the current full model and the simplified model of isothermal solidification for the evolution of the liquid layer half-width versus bonding time during TLP bonding of the Au/Sn system. A small 'sensible mass density' interval of 1.0×10^{-4} g/cm^3 and a grid system of 1,100 nodes are employed for the full model, whilst a dimensionless small 'sensible mass density' interval, $\Delta d'$, of 1.0×10^{-6} and a grid system of 1,100 nodes are employed for the simplified model

model for describing the TLP bonding process of two-phase systems with a moving solid–liquid interface.

Conclusions

The fixed-grid source-base method has been successfully adopted to model TLP bonding and other diffusion-controlled phase change processes. The model was developed by introducing the 'sensible mass density' and 'latent sensible mass density of phase change' to merge the diffusion equations for the two phases and the moving interface into one unique diffusion equation. Important issues include using a sufficient small 'sensible mass density' interval to describe the diffusion-controlled phase change, and updating the diffusion coefficient around the moving interface using the harmonic mean, rather than the arithmetic mean of the values for the two phases.

Under the assumption of constant Molar volume, the current fixed-grid source-based model can produce predictions in good agreement with those predicted from Illingworth et al.'s variable grid model for the evolution of liquid layer half-width against bonding time during TLP bonding of the Ni/Ni–P system and of the interface displacement against processing time during solid state diffusion of α-brass/β-brass system. In comparison with Illingworth et al.'s model, the current fixed-grid source-based model is more conveniently and simply extended to multi-component, multi-phase and high-dimensional problems. By assuming 50% reduction in Molar volume of phosphorous, the current model further improves the prediction of the evolution of liquid layer half-width against bonding time during TLP bonding of the Ni/Ni–P system compared to the experimental results.

The current model can overcome the problems associated with the convergence of calculation and conservation of solute in the previous fixed-grid models, without the need for a complicated formulation describing the moving interface. The current model predicts significantly shorter bonding times for the liquid layer to disappear than Cain et al.'s fixed-grid model for the TLP bonding of Au/Sn. This is probably associated with the fact the numerical scheme in Cain et al.'s model was physically unrealistic, and hence introduced significant errors.

The current model can be further approximated to a simplified model of the isothermal solidification for parametric analysis during TLP bonding. The relevant formulation indicates that the process of isothermal solidification can be expressed as a function of only a sub-saturation parameter and a geometric parameter. The diffusion coefficient and the initial thickness of the liquid layer affect the solidification in a self-similar manner. The solidification time increases linearly with increasing diffusion coefficient, and parabolically with increasing initial liquid layer thickness. The solidification times predicted using the current simplified solidification model are also in good agreement with those predicted from Illingworth et al.'s variable model for different sub-saturation and geometric parameters.

Acknowledgements This research was funded by the Engineering and Physical Science Research Council and the Innovative Electronic Manufacturing Research Centre in the UK.

References

1. MacDonald WD, Eagar TW (1992) In: Cieslak MJ, Perepezko JH, Kang S, Glicksman ME (eds) The metal science of joining. The Minerals, Metal & Matreials Society, Warrendale, PA, p 93
2. MacDonald WD, Eagar TW (1992) Annu Rev Mater Sci 22:23
3. Bernstein L (1966) J Electrochem Soc 113(12):1282
4. Roman JW, Eagar TW (1992) Proceedings of the 1992 international symposium on microelectronics, IMPAS, p 52
5. Cain SR, Wilcox JR, Venkatraman R (1997) Acta Mater 45(2): 701
6. Chuang RW, Lee CC (2002) IEEE T Compon Pack T 25(3):453
7. Humpston G, Jacobson DM (2004) Principles of soldering, ASM International, Materials Park, Ohio 44073-0002, p 230
8. Bosco NS, Zok FW (2004) Acta Mater 52(10):2965
9. Bosco NS, Zok FW (2005) Acta Mater 53(7):2019
10. Heckel RW, Hickl AJ, Zaehring RJ, Tanzilli RA (1972) Metall Trans 3(10):2565
11. Zhou Y, North TH (1993) Model Simul Mater Sci 1(4):505
12. Nakagawa H, Lee CH, North TH (1991) Metall Trans A 22A(2):543
13. Sinclair CW, Purdy GR, Morral JE (2000) Metall Mater Trans A 31A(4):1187

14. Campbell CE, Boettinger WJ (2000) Metall Mater Trans A 31A(11):2835
15. Zhou Y (2001) J Mater Sci Lett 20(9):841
16. Shinmura T, Ohsasa K, Narita T (2001) Mater Trans 42(2):292
17. Illingworth TC, Golosnoy IO, Gergely V, Clyne TW (2005) J Mater Sci 40(9/10):2505. doi:10.1007/s10853-005-1983-y
18. Illingworth TC, Golosnoy IO, Clyne TW (2007) Mat Sci Eng A-Struct A445-A446: 493
19. Kajihara M (2009) J Mater Sci 44(8):2109. doi:10.1007/s10853-009-3299-9
20. Di Luozzo N, Fontana M, Arcondo B (2007) J Mater Sci 42(11): 4044. doi:10.1007/s10853-006-0190-9
21. Voller VR, Prakash C (1987) Inter J Heat Mass Trans 30(8):1709
22. Brent AD, Voller VR, Reid KJ (1988) Numer Heat Trans 13:297
23. Voller VR, Swaminathan CR (1991) Numer Heat Trans B-Fund 19:175
24. Dutta P, Joshi Y, Janaswamy R (1995) Numer Heat Trans A-Appl 27:499
25. Chakraborty S, Dutta P (2001) Metall Mater Trans B 32B:562
26. Kumar A, Dutta P (2009) J Mater Sci 44(15):3952. doi: 10.1007/s10853-009-3539-z
27. Patankar SV (1980) Numerical heat transfer and fluid flow. Hemisphere, Washington, DC, p 41
28. The Numerical Database DETHERM, Available from: http://www.dechema.de/detherm-lang-en
29. Lee CC, Wang CY (1992) Thin Solid Films 208(2):202
30. German R, Suri P, Park S (2009) J Mater Sci 44(1):1. doi: 10.1007/s10853-008-3008-0
31. McKenna IM, Gururajan MP, Voorhees PW (2009) J Mater Sci 44(9):2206. doi:10.1007/s10853-008-3196-7